

MASTERING ROBOT MANIPULATION WITH MULTIMODAL PROMPTS THROUGH PRETRAINING AND MULTI-TASK FINE-TUNING

Anonymous authors

Paper under double-blind review

ABSTRACT

Prompt-based learning has been demonstrated as a compelling paradigm contributing to large language models' tremendous success (LLMs). Inspired by their success in language tasks, existing research has leveraged LLMs in embodied instruction following and task planning. However, not much attention has been paid to embodied tasks with multimodal prompts, combining vision signals with text descriptions. This type of task poses a major challenge to robots' capability to understand the interconnection and complementarity between vision and language signals. In this work, we introduce an effective framework that learns a policy to perform robot manipulation with multimodal prompts from multi-task expert trajectories. Our methods consist of a two-stage training pipeline that performs inverse dynamics pretraining and multi-task finetuning. To facilitate multimodal understanding, we design our multimodal prompt encoder by augmenting a pre-trained LM with a residual connection to the visual input and model the dependencies among action dimensions. Empirically, we evaluate the efficacy of our method on the VIMA-BENCH (Jiang et al., 2023) and establish a new state-of-the-art (10% improvement in success rate). Moreover, we demonstrate that our model exhibits remarkable in-context learning ability.

1 INTRODUCTION

The unprecedented advancement of large language models (LLM) (Brown et al., 2020; OpenAI, 2023; Chowdhery et al., 2022; Anil et al., 2023; Chung et al., 2022; Touvron et al., 2023) has stimulated rapid development of building instruction-following agents (Lynch & Sermanet, 2020; Ahn et al., 2022; Driess et al., 2023; Guhur et al., 2023; Huang et al., 2022a). By leveraging LLM's remarkable zero-shot generalizability, various research initiatives Ahn et al. (2022); Huang et al. (2022a;b) have developed powerful action planners to parse language instructions into a sequence of sub-goals. A prominent example is the SayCan (Ahn et al., 2022), which employs PALM (Chowdhery et al., 2022) to transform abstract task descriptions into actionable step-by-step plans.

However, relying solely on language instructions can be inefficient for describing intricate task details. For instance, directing a household robot to tidy out a living room is more straightforward with a combination of language and visual cues than using language alone. Also, when learning new tasks, words simply cannot convey as much information as video demonstrations (Dasari & Gupta, 2021). In addition, human communication is inherently multimodal, often combining speech with expressive gestures and demonstrations (Drijvers & Holler, 2023). Therefore, we are motivated to enhance a robot's comprehension of multimodal task prompts that interleave text and images.

Training a robot to interpret multimodal prompts presents several challenges. The vision signals in the prompt may simply represent target objects, delineate a specific sub-goal, or offer in-context demonstrations. Here, the robot must first understand the underlying transition dynamics suggested by the multimodal prompts before tackling the overall task objective. This requires the robot to infer state transitions from language instructions, and also to be capable of inferring actions from image signals, i.e., inverse dynamic prediction. Furthermore, it is essential for the robot to pay attention to critical visual details, such as the orientation of an object shown in the image, as this can significantly influence its action prediction.

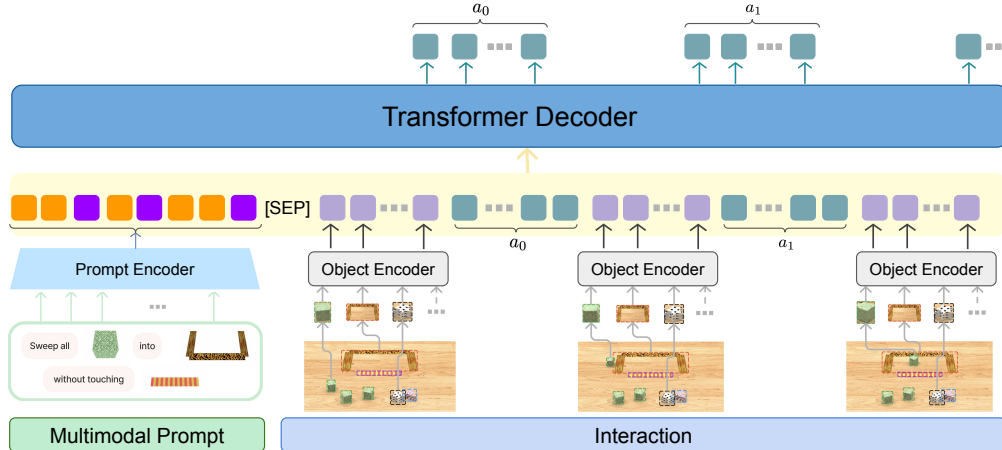


Figure 1: **Model Architecture.** Our model adopts a decoder-only architecture. The multimodal prompt embeddings are concatenated with history tokens. We model each action dimension as an individual token and predict them auto-regressively.

Matching object appearance with textual representation can be achieved by multi-task imitation learning on a diverse set of tasks (Jiang et al., 2023). However, this method falls short in teaching robots to predict inverse dynamics due to the masking of future observations in multi-task imitation learning. To overcome this challenge, we introduce a two-stage training pipeline: inverse dynamic pretraining and multi-task finetuning (FT). Our pretraining strategy first converts any robot trajectory into a motion-following task and then trains the robot to recover the action sequences given the observed image sequence. To capture fine-grained visual information, we design our multimodal prompt encoder by augmenting a pretrained LM with a residual connection (RC) adding from the input visual tokens to the encoded embeddings of the LM.

Figure 1 provides an overview of our model, which adopts a decoder-only architecture (Radford et al., 2018). Specifically, we model each action dimension as individual action token and predict them auto-regressively to capture dependencies among different dimensions. We dub our method as **Multi-modal Inverse Dynamics AgentS (MIDAS)**. Empirically, we evaluate our method on the VIMA-BENCH (Jiang et al., 2023) and establish a new state-of-the-art, outperforming VIMA by $\sim 10\%$ on all 4 evaluation protocols of VIMA-BENCH. Furthermore, we showcase the our multi-task policy’s superior in-context learning ability by modifying the original VIMA-BENCH. **We emphasize this is novel, as simultaneously equipping a robot with multi-task and in-context learning abilities has not been extensively explored.**

In summary, our contributions can be summarized as follows:

- Introduction of the two-stage MIDAS training framework, which establishes a new state-of-the-art on VIMA-BENCH (Jiang et al., 2023).
- An effective multimodal prompt encoder that can capture visual and textual details.
- Empirically highlighting the superior in-context learning ability of our multi-task policy.

2 PRELIMINARY

Problem Definition We consider the problem of learning a multimodal prompt-conditioned policy $\pi : \mathcal{P} \times \Omega \rightarrow \mathcal{A}$ that maps the multimodal prompt $q \in \mathcal{P}$ and the history trajectory $\omega_t = (o_0, a_0, o_1, \dots, a_{t-1}, o_t) \in \Omega$ to the two-pose action primitive (Zeng et al., 2021) $a_t = (\mathcal{T}_{\text{initial}}, \mathcal{T}_{\text{target}}) \in \mathcal{A} \subseteq \mathcal{R}^{N_a}$, where $o_t \in \mathcal{O}$ denotes the visual observation at timestep t and N_a denotes the number of action dimensions.

$$\pi(q, \omega_t) = \pi(q, o_0, a_0, o_1, \dots, a_{t-1}, o_t) \rightarrow a_t = (\mathcal{T}_{\text{initial}}, \mathcal{T}_{\text{target}}) \in \mathcal{A} \subseteq \mathcal{R}^{N_a} \quad (1)$$

The action space \mathcal{A} consists of primitive motor skills like “pick and place” and “push”. For the “pick and place” primitive, $\mathcal{T}_{\text{initial}}$ and $\mathcal{T}_{\text{target}}$ defines the space of pick pose and place pose, respectively.

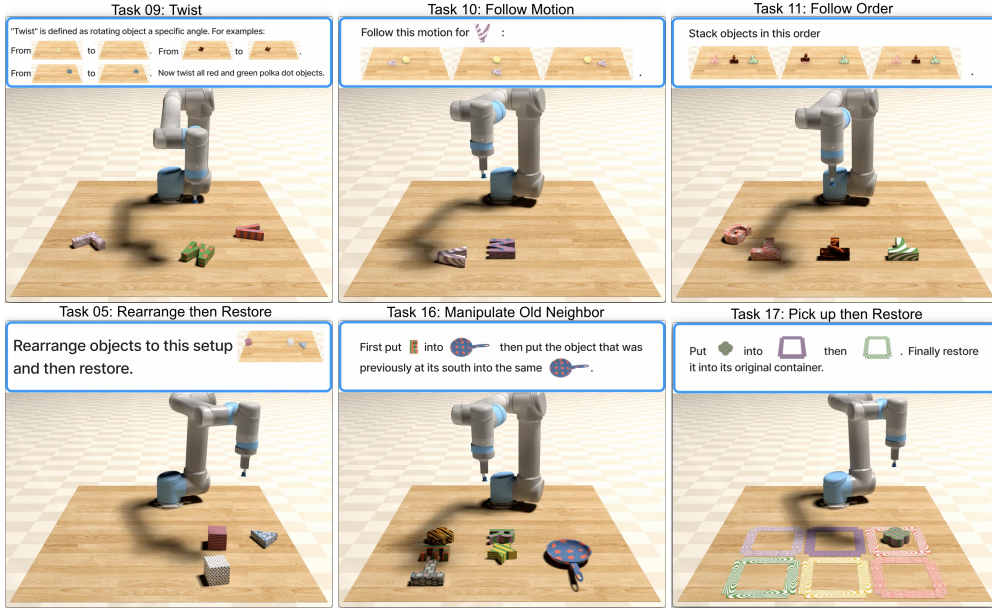


Figure 2: Task samples from the VIMA-BENCH. We refer readers to Appendix B of the VIMA paper (Jiang et al., 2023) for detailed task description.

For “push”, they define the space of the starting and ending pose of push. The multimodal prompt describes the task goal by interleaving texts and images.

In this paper, we aim to learn a multi-task policy π_θ parameterized by θ from a dataset $\mathcal{D} = \{\zeta_1, \dots, \zeta_N\}$ with N expert demonstration. Each training sample $\zeta_i = (q^i, \omega^i)$ contains the expert trajectory $\omega^i = (o_0^i, a_0^i, o_1^i, \dots, a_{T-1}^i, o_T^i)$ corresponding to the multimodal task prompt q_i .

VIMA policy Jiang et al. (2023) propose the VisuoMotor Attention (VIMA) agent to solve robot manipulation from multimodal prompts with a Transformer (Vaswani et al., 2017) Encoder-Decoder architecture. It encodes the multimodal prompts that interleave textual and visual tokens with a pre-trained LM by following the practice of Frozen (Tsimpoukelli et al., 2021). Its autoregressive action decoding is conditioned on the prompt embedding via cross attention layers that alternate with the causal self-attention. Instead of directly operating on the raw RGB images, VIMA adopts the object-centric representation by cropping objects from both prompt and observation images and forming them as a sequence of object tokens with pixel coordinate information as shown in Figure 3a. Notably, VIMA predicts each action dimension independently and trains its model via behavior cloning with the loss function for a trajectory with T steps given by

$$L(\theta) = -\min_{\theta} \sum_{t=0}^{T-1} \log \pi_{\theta}(a_t | q, \omega_t) = -\min_{\theta} \sum_{t=0}^{T-1} \sum_{n=0}^{N_a-1} \log \pi_{\theta}(a_t^n | q, \omega_t). \quad (2)$$

We build our policy upon the VIMA policy. However, we model the dependencies among different action dimensions (Giuliani et al., 2021; Vinyals et al., 2019) and decode each dimension autoregressively. We detail our motivation in Sec. 3.3 and demonstrate its empirical benefit in Sec. 4.

VIMA-BENCH (Jiang et al., 2023) is built on top of the Ravens (Zeng et al., 2021; Shridhar et al., 2023) simulator and contains 17 types of tabletop manipulation tasks. Figure 2 shows 6 representative tasks from the VIMA-BENCH. Each task type can instantiate thousands of individual task instances by combining various textures and objects. Specifically, each task instance defines a multimodal prompt that interleaves texts and images and the type of end-effector $\in \{\text{suction cup, spatula}\}$. The suction cup corresponds to the primitive motor skill “pick and place” while spatula corresponds to “wipe”. At each time step, the agent receives RGB images rendered from both frontal and top-down views and predicts the initial and target pose of its end effector.

VIMA-BENCH establishes a four-level protocol to evaluate progressively stronger generalization, ranging from placement generalization (L1), combinatorial generalization (L2), novel task general-



Figure 3: (a) **Object Encoder** proposed in VIMA consists of a ViT (Dosovitskiy et al., 2020) that extracts visual embedding from cropped object images and a MLP that encodes bounding boxes. The two embeddings are concatenated before passing through a Fusion MLP to get the object tokens. (b) **Multimodal Prompt Encoder** adds a RC from the input object tokens to the pretrained LM output.

ization (L3) and novel task generalization (L4). Expert demonstration are provided for 13 tasks as the training data, with 50K trajectories per task. The other 4 tasks are included into the L4 task suite.

3 METHODS

We introduce our MIDAS framework that learns a multi-task policy to perform robot manipulation with multimodal prompt. We propose a two-stage training pipeline that includes inverse dynamic pretraining (Sec. 3.1) followed by multi-task FT. To capture fine-grained visual information, we design our multimodal prompt encoder by augmenting a pretrained LM with a residual connection to the input object token (Sec. 3.2). Moreover, we model each action dimension as an individual action token and autoregressively decodes each dimension (Sec. 3.3). Sec. 3.4 summarizes our training framework, with an overview of our model architecture given in Figure 1.

3.1 PRETRAINING TASK: INVERSE DYNAMICS PREDICTION

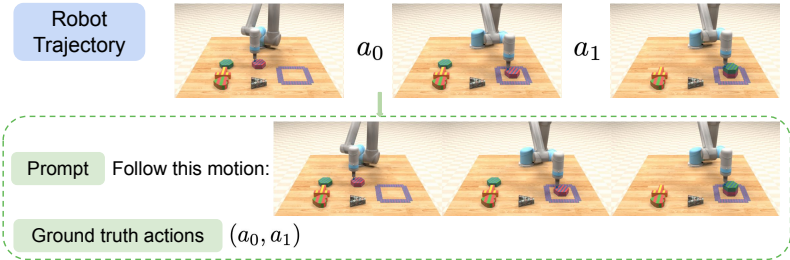


Figure 4: Given the any sequence of robot trajectory, we can always formulate a motion following task that requires the agent to replicate the demonstration trajectory.

As mentioned in Sec. 1, images in the prompt can depict object appearance, appearances, outline the sub-goals and success criteria of a task, or serve as in-context task demonstrations. To decipher this underlying task information and learn from in-context examples, a robot needs to understand the transition dynamics illustrated in a sequence of images. For instance, the robot should be able to infer the action sequence required to transition from its current state to the target goal state.

In other words, the agent needs proficiency in inverse dynamics prediction. Given a sequence of observations (o_0, \dots, o_T) , the robot should learn to infer the corresponding action sequence (a_0, \dots, a_{T-1}) . However, the skill cannot be directly acquired by imitating multi-task trajectories, as future observations are often masked out when predicting actions with current observations.

To tackle the dilemma, we make a novel observation that every robot trajectory itself can be reformulated into a motion following task. As shown in Figure 4, given any sequence of robot trajectory

$\omega_T = (o_0, a_0, o_1, \dots, a_{T-1}, o_T)$, we can always create a task with the prompt *Follow this motion:* o_0, \dots, o_T and ground-truth actions (a_0, \dots, a_{T-1}) , leading to the following pretraining loss

$$L_{\text{pretrain}}(\theta) = -\min_{\theta} \sum_{t=0}^{T-1} \log \pi_{\theta}(a_t | \text{Follow this motion: } o_0, \dots, o_T; \omega_t) \quad (3)$$

3.2 MULTI-MODAL PROMPT ENCODING

To capture visual and textual information from the multimodal prompt, VIMA proposes to encode both the visual and language tokens in the prompt with a pretrained LM (T5-base) following the practice of Frozen (Tsimpoukelli et al., 2021). While LLM has demonstrated a tremendous success across various fields with superior generalizability (Li et al., 2022), our early experiments reveal that this encoding strategy often fails to capture some fine-grained visual information, e.g., the rotation angle of an object (Task 09, Figure 2). We hypothesize it is because the pretrained LM has never been trained on visual data.

To overcome this challenge, we propose to augment the pretrained LM by adding a residual connection (RC) from the input visual tokens to the encoded embeddings, as shown in Figure 3b. The intuition is that by directly adding the original visual tokens to the embeddings produced by the pretrained LM, we can retain more detailed visual information that might be lost during the encoding process. Our experiments in Sec. 4 validate this intuition, showing that the inclusion of the RC significantly improves performance across different tasks.

3.3 MODELING THE DEPENDENCY AMONG EACH ACTION DIMENSION

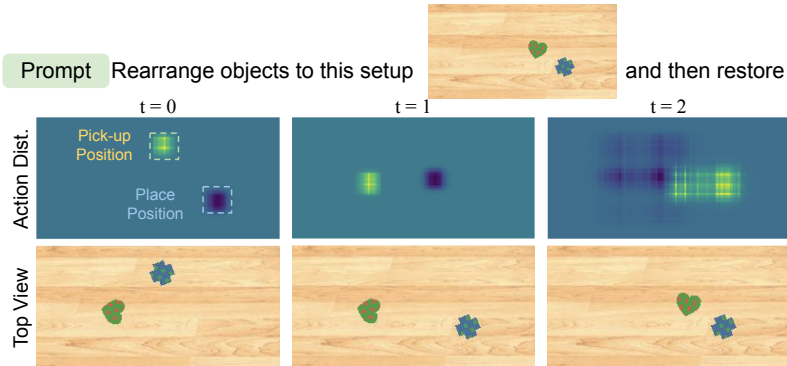


Figure 5: At $t = 2$, the robot can choose to move either the heart or the cross block. As the policy predicts each action dimension independently, different dimensions do not consistently manipulate the same object, resulting in a task failure.

Recall that the robot action is defined by the initial pose $\mathcal{T}_{\text{initial}}$ and target pose $\mathcal{T}_{\text{target}}$ of the end effector. Intuitively, $\mathcal{T}_{\text{target}}$ should depend on $\mathcal{T}_{\text{initial}}$. And thus independently predicting each action dimension can be problematic. Consider the example in Figure 5, the robot is tasked to first rearrange the objects to a desired arrangement and then restore them to original setup. When the robot begins to restore at $t = 2$, it has the option to move either the heart or the cross block. As the policy predicts each action dimension independently, the dimensions associated with the pick-up pose do not align consistently with one specific object. Consequently, the distribution of pick-up position assigns significant probability to both object locations. Similarly, the placement position distribution allocates probability to both objects’ target positions. When sampling actions from this distribution, the robot may either miss picking up an object or misplace it, leading to a task failure.

Therefore, we opt to model the dependency among action dimensions by modeling each dimension as a single token and decode each token autoregressively as shown in Figure 1. And thus, the multi-task imitation loss function can be reformulated into

$$L_{\text{Imitation}}(\theta) = -\min_{\theta} \sum_{t=0}^{T-1} \left(\log \pi_{\theta}(a_t^0 | q, \omega_t) + \sum_{n=1}^{N_a-1} \log \pi_{\theta}(a_t^n | q, \omega_t, a_t^0, \dots, a_t^{n-1}) \right). \quad (4)$$

Table 1: We compared our methods with baseline approaches on the VIMA-BENCH across all four evaluation levels. ‘‘Avg’’ represents the average success rate for all tasks within an evaluation level. To determine the success rate for each method, we sampled 200 episodes from every task. Due to limited space, we report the success rate for four representative tasks in this table. Full results can be found in Appendix A. Our methods significantly outperform baseline methods and establish a new state-of-the-art performance on the VIMA-BENCH.

Method	L1					L2					L3					L4	
	Avg	T5	T9	T16	T17	Avg	T5	T9	T16	T17	Avg	T5	T9	T16	T17	Avg	T10
Gato	57.0	44.5	14.0	43.0	1.5	53.9	46.0	10.5	42.0	1.0	45.6	36.0	17.0	41.5	0.0	13.5	0.0
Flamingo	47.2	41.0	3.0	38.0	2.0	47.1	43.0	4.5	40.0	1.0	42.1	36.5	6.0	45.5	0.5	11.1	0.0
GPT	47.9	45.0	8.0	33.0	1.0	47.4	43.0	10.5	34.0	3.0	42.6	32.0	5.0	37.5	0.0	12.1	0.5
VIMA	87.2	65.0	13.5	88.0	77.0	87.0	61.0	12.5	87.5	77.5	84.0	63.0	12.0	58.5	78.0	49.6	0.0
Gato OBJ	87.5	62.0	17.0	92.5	80.5	87.5	62.5	16.0	91.5	80.0	84.4	65.5	15.5	46.5	87.5	49.6	0.0
Ours																	
w/o Pretrain	91.6	88.0	20.5	93.0	98.0	91.8	87.0	23.5	92.0	98.0	88.3	90.0	20.5	50.5	99.5	49.1	0.0
w/ Pretrain	97.8	94.0	100	94.0	96.5	97.9	96.5	100	93.0	96.0	93.4	94.0	97.0	47.0	98.0	59.1	41.0

That is, the distribution for each action dimension should be conditioned on the other action dimensions that have already been decoded.

3.4 ALGORITHM SUMMARY

To this end, we have introduced our pretraining strategies and model design. To learn our multi-task policy π_θ , we assume the access to a dataset $\mathcal{D} = \{\zeta_1, \dots, \zeta_N\}$ with N expert demonstration. First, we pretrain π_θ by minimizing $L_{\text{pretrain}}(\theta)$ over N_{pretrain} iterations. Subsequently, we perform multi-task fine-tuning on \mathcal{D} to minimize $L_{\text{imitation}}(\theta)$. The pseudo-codes (Algorithm 1) and detailed hyper-parameters (HP) are available in Appendix B.

4 EXPERIMENTAL RESULTS

Our experiments focus on the VIMA-BENCH (Jiang et al., 2023), addressing two primary questions: 1) Does our model design and training pipeline enhance the zero-shot generalization of the learned model? 2) Can our model effectively utilize in-context examples to tackle novel tasks? To answer the first question, we evaluate our methods on the VIMA-BENCH (Sec. 4.1) and conduct extensive ablation studies (Sec. 4.2). To answer the second question, we modify the VIMA-BENCH by holding out more tasks with in-context examples from the training set to test our methods (Sec. 4.3).

4.1 STANDARD EVALUATION ON THE VIMA-BENCH

We compare our methods with various baselines from the original VIMA paper (Jiang et al., 2023) on the VIMA-BENCH. All baseline methods only conduct multi-task imitation learning without pretraining. We directly report results for Gato (Reed et al., 2022), Flamingo (Alayrac et al., 2022) and GPT (Radford et al., 2018) from the VIMA paper. Notably, these three methods directly operate on the raw image observation. In contrast, VIMA, Gato OBJ and our methods adopt an object-centric representation. The Gato OBJ policy is constructed by replacing the encoder-decoder architecture of the VIMA policy with a decoder-only architecture (Radford et al., 2018). And the difference between our policy and Gato OBJ is that we augments the pretrained LM with a RC and model each action dimension as an individual action token. As we do not focus on the visual understanding part of general robot control, we assume the access to the ground truth instance segmentation masks provided by the VIMA-BENCH for all methods with an object-centric representation. And the results of VIMA and Gato OBJ are reproduced by us.

Table 1 presents the evaluation results by following VIMA-BENCH’s 4-level evaluation protocols. Due to the limited space, we only report the individual task success rates for representative tasks on which different methods exhibit a significant performance difference. Avg denotes the task success rate across all tasks from an evaluation level. Full evaluation results with individual task success rate can be found in Appendix A. We can observe that our methods already outperforms all baseline methods even without pretraining, particularly on Task 5 (*Rearrange the Restore*) and Task 17 (*Pick up then Restore*), which demonstrates the effectiveness of our multimodal prompt encoder and the

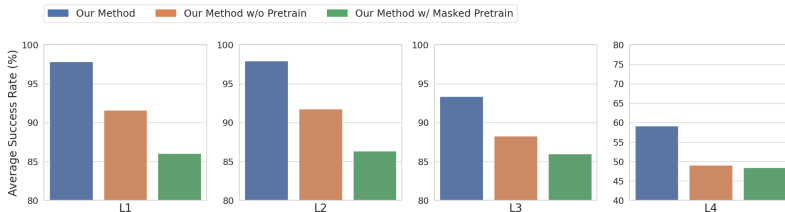


Figure 6: Ablation study on the pretraining strategy. We show that the BERT-style pretraining strategy (Our Method w/ Masked Pretrain) that performs masked action modeling does not benefit the learning of a multi-task policy to understand multimodal prompts.

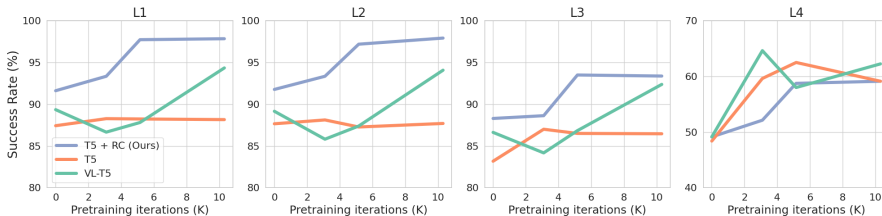


Figure 7: Ablation on the prompt encoder. We compare the performance of our methods with different prompt encoders. Our proposed T5 + RC prompt encoder that augments a pretrained T5 with a residual connection (RC) to the input visual tokens achieves a higher computational efficiency by requiring less pretraining iterations to reach a decent performance on L1, L2, and L3.

importance of modeling the dependencies between initial and target pose of the action. With pretraining, the performance of our methods improves significantly, especially on the difficult Task 9 (*Twist*) and Task 10 (*Follow Motion*). As shown in Figure 2, *Twist* requires the robot to first deduce the target rotation angles from the in-context examples before operating on the correct objects described by text. Similarly, *Follow Motion* requires the robot to deduce the actions corresponding to the image sequence in the prompt and apply them to the same object in robot’s current observation. Without pretraining, models have to learn the skills for inverse dynamics prediction solely from the multi-task data, lacking enough supervision.

4.2 ABLATION STUDIES

We conduct extensive experiments to study how our model design and training pipeline impacts the robot manipulation, focusing on the effectiveness of our pretraining strategy and prompt encoding. We also examine the impact of data scaling and model size. Appendix A presents individual task success rate for all methods and further ablate the decoder-only architecture of our model.

Pretraining Strategy Figure 6 compared our pretraining strategy with a BERT-style masking prediction method (Devlin et al., 2018), which still performs the task of inverse dynamics prediction. Specially, we modify the decoding mask of the transformer to allow its attention to all future observation but mask all prompt and future action tokens. However, this pretraining strategy does not benefit the downstream multitask learning, as it does not explicitly train the model to reason the image sequences presented in the prompt.

Multimodal Prompt Encoding Recall that our multimodal prompt encoder (T5 + RC) augments a pretrained LM (T5-Base (Raffel et al., 2020)) with a RC to the input visual tokens. To investigate its efficacy, we compare its performance with two variants that respectively adopt a pretrained T5 and VL-T5 (Cho et al., 2021) to encode the multimodal prompt. Note that T5 is pretrained on pure text data while VL-T5 is pretrained on both vision and language data. As shown in Figure 7, our method achieves an overall better performance and computational efficiency by requiring less pretraining iterations. The comparison between the performance of T5 and VL-T5 shows that a pretrained encoder that better understands input visual tokens can benefit more from our pretraining phase.

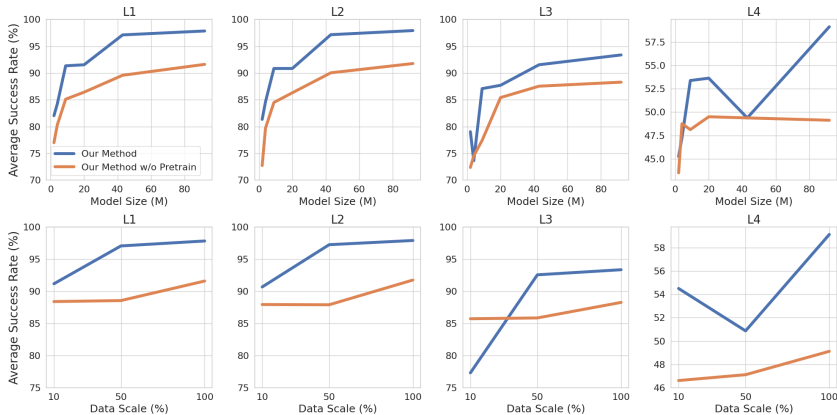


Figure 8: Ablation on model and data sizes. *Top*: For model sizes ranging from 2M to 92M, our pretraining can always learn a representation that leads to better multitask performance. *Bottom*: Model size is fixed to 92M. The benefit of pretraining increases as we increase training data size.

Model & Data Scalability Figure 8 illustrates the performance of our methods in relation to variations in model and data size. As the model size is scaled from 2M to 92M, we maintain a constant prompt encoder and exclude it from the parameter count, adhering to VIMA practices. Conversely, while adjusting the data size, the model remains fixed at 92M, and performance is evaluated using 10%, 50%, and 100% of the data available in VIMA-BENCH. Notably, the enhancements derived from our pretraining remain evident in low parameter regime. Additionally, a larger dataset correspondingly amplifies the performance gains achieved through our pretraining techniques.

4.3 EVALUATING THE IN-CONTEXT LEARNING ABILITY

Previous experiments already demonstrate the superior generalizability of our methods on L1, L2 and L3, which differs from the training tasks in object placement, combination and types. When exposed to novel tasks from L4, we expect our framework imbues the agent with a human-like intuition to learn from in-context examples. This expectation holds even if none of the training tasks explicitly present few-shot demonstrations within their prompts. To access this capability, we modify the original VIMA-BENCH by carefully constructing a new set of L4 tasks, ensuring each of the L4 tasks contain in-context examples in the prompt. Specifically, we hold out *Twist* and *Follow Order* from the training tasks, combining them with *Follow Motion* to form the new L4 task suites. The first row of Figure 2 showcases samples from these designated tasks.

As L4 tasks contain novel scenes/objects that does not exist in the training data, we leverage data augmentation during pretraining phase to improve model generalizability. Additionally, we propose *Modified FT* that randomly replace the object image in the prompt with text description provided by the VIMA-BENCH during multi-task finetuning. At inference time, we edit the prompt of *Twist* and *Follow Order* to make them closer to the pretraining prompt without adding extra task information. Appendix C provides detailed experiment setup.

As shown in Table 2, our method considerably outperforms baseline methods for the *Twist* and *Follow Motion* without decreasing its performance on L1, L2 and L3 (shown in Appendix C). *Twist* requires the model to first infer the rotation angle from prompt image sequence and then identify the target object described with text. While the imitation-learned policy (Our Method w/o Pretrain) shows limited performance on these tasks, our pretrained policy (Our Method w/ Pretrain Only) exhibits some capability, particularly in *Follow Order* which does not necessitate understanding object descriptions. However, it has difficulties with *Twist* and *Follow Motion* because it has never trained to tackle the visual and textual object. In contrast, the multi-task FT phase helps the model to understand diverse multimodal prompts and solicit its ability to translate action sequences derived from in-context examples to target objects. This is akin to the improvement seen in pretrained language models’ instruction following abilities due to instruction-fining, as highlighted by (Sanh et al., 2021;

Table 2: Evaluating the in-context learning capability of the learned model. We hold out *Twist* and *Follow Order* from the training data.

Task	T9: Twist	T10: Follow Motion	T11: Follow Order	Overall
Our Method	26.5%	74.0%	8.0 %	36.2%
Our Method w/o Modified FT	10.0%	43.5 %	16.5%	23.3%
Our Method w/ Pretrain Only	8.0 %	2.0%	15.5 %	8.5 %
Our Method w/o Pretrain	1.5 %	0.5 %	0.0%	0.7 %

Ouyang et al., 2022; Wei et al., 2021). Moreover, our Modified FT significantly improves model’s grounding capability, contributing to a remarkable performance increase in *Twist* and *Follow Motion*.

[Appendix D provides additional results, where we design 4 new tasks with in-context examples in the prompt to solidify our findings.](#)

5 RELATED WORK

Multi-Task Pretraining via Sequence Modeling. The development of the Transformer architecture (Vaswani et al., 2017) paved the way for large-scale pretraining, which has become a standard practice to enable better generalization across different domains (Brown et al., 2020; Chen et al., 2021; Radford et al., 2021; Devlin et al., 2018; Lu et al., 2022). Specifically, these models employ the *sequential modeling* (Sutskever et al., 2014) techniques to capture temporal dependencies in the data. By training on massive web-scale data, the trained models demonstrate emergent behaviors (Brown et al., 2020; Chowdhery et al., 2022; Touvron et al., 2023), e.g., the ability to perform in-context learning. While multi-task pretraining has been extensively employed in natural language processing (NLP) and computer vision (CV), its applications in robotic systems are also gaining increasing attention (Driess et al., 2023; Brohan et al., 2022; 2023; Radosavovic et al., 2023). In our work, we pretrain our model by converting diverse robot trajectories into inverse dynamics prediction tasks, facilitating the in-context learning and multi-task performance of the our learned model.

Multimodal Learning. The field of multimodal learning, which focuses on integrating data from various modalities, has seen remarkable advancements (Radford et al., 2021; Wang et al., 2022; Jaegle et al., 2021). Flamingo, for instance, trains a model to generate textual completion based on multimodal prompts (Alayrac et al., 2022). The Perceiver framework (Jaegle et al., 2021) offers an adaptable method to process structured input and output. Moreover, Gato (Reed et al., 2022) introduces a versatile agent proficient in NLP, CV, and robotics. [Our research tackles robot manipulation given interleaved image and text task prompt.](#) Concurrently, MUTEX (Shah et al., 2023) learns a policy to tackle task prompts from multiple modalities (image, video, text, and speech).

Inverse Dynamics Modeling (IDM) for Representation Learning. IDM has proved to be an effective approach for learning from high-dimensional demonstration data. Training the model on an IDM task of predicting the agent’s actions given the high-dimensional observations allows effective learning of a feature space that represents only the information relevant to the actions (Brandfonbrener et al., 2023). Pathak et al. (2017) uses IDM to generate intrinsic reward signals with self-supervision for efficient exploration. Efroni et al. (2021); Lamb et al. (2022) use a multi-step inverse dynamics model to enable representation learning robust to exogenous information. Most recently, Baker et al. (2022); Venuto et al. (2023); Thomas et al. (2023) use IDM for data-efficient multi-task pre-training on complex sequential decision-making domains. Our method leverages IDM to facilitate robot’s in-context learning capability and its understanding on the transition dynamics.

6 CONCLUSION

In this paper, we introduce our MIDAS framework that trains a robot to comprehend multimodal prompts. The pretraining phase trains the agent to perform inverse dynamics prediction, facilitating robot’s understanding of transition dynamics. To capture fine-grained visual information from the prompt images, we augment a pretrained LM with a RC to the object token. We further model the dependency among different action dimensions. Empirically, we establish a new state-of-the-art on the VIMA-BENCH and also demonstrate the in-context learning capability of our learned policy.

REPRODUCIBILITY STATEMENT

We are going through internal code review and will open source our codes once it gets approved.

REFERENCES

- Michael Ahn, Anthony Brohan, Noah Brown, Yevgen Chebotar, Omar Cortes, Byron David, Chelsea Finn, Chuyuan Fu, Keerthana Gopalakrishnan, Karol Hausman, Alex Herzog, Daniel Ho, Jasmine Hsu, Julian Ibarz, Brian Ichter, Alex Irpan, Eric Jang, Rosario Jauregui Ruano, Kyle Jeffrey, Sally Jesmonth, Nikhil Joshi, Ryan Julian, Dmitry Kalashnikov, Yuheng Kuang, Kuang-Huei Lee, Sergey Levine, Yao Lu, Linda Luu, Carolina Parada, Peter Pastor, Jornell Quiambao, Kanishka Rao, Jarek Rettinghouse, Diego Reyes, Pierre Sermanet, Nicolas Sievers, Clayton Tan, Alexander Toshev, Vincent Vanhoucke, Fei Xia, Ted Xiao, Peng Xu, Sichun Xu, Mengyuan Yan, and Andy Zeng. Do as i can and not as i say: Grounding language in robotic affordances. In *arXiv preprint arXiv:2204.01691*, 2022.
- Jean-Baptiste Alayrac, Jeff Donahue, Pauline Luc, Antoine Miech, Iain Barr, Yana Hasson, Karel Lenc, Arthur Mensch, Katherine Millican, Malcolm Reynolds, et al. Flamingo: a visual language model for few-shot learning. *Advances in Neural Information Processing Systems*, 35:23716–23736, 2022.
- Rohan Anil, Andrew M Dai, Orhan Firat, Melvin Johnson, Dmitry Lepikhin, Alexandre Passos, Siamak Shakeri, Emanuel Taropa, Paige Bailey, Zhifeng Chen, et al. Palm 2 technical report. *arXiv preprint arXiv:2305.10403*, 2023.
- Bowen Baker, Ilge Akkaya, Peter Zhokov, Joost Huizinga, Jie Tang, Adrien Ecoffet, Brandon Houghton, Raul Sampedro, and Jeff Clune. Video pretraining (vpt): Learning to act by watching unlabeled online videos. *Advances in Neural Information Processing Systems*, 35:24639–24654, 2022.
- David Brandfonbrener, Ofir Nachum, and Joan Bruna. Inverse dynamics pretraining learns good representations for multitask imitation. *arXiv preprint arXiv:2305.16985*, 2023.
- Anthony Brohan, Noah Brown, Justice Carbajal, Yevgen Chebotar, Joseph Dabis, Chelsea Finn, Keerthana Gopalakrishnan, Karol Hausman, Alex Herzog, Jasmine Hsu, et al. Rt-1: Robotics transformer for real-world control at scale. *arXiv preprint arXiv:2212.06817*, 2022.
- Anthony Brohan, Noah Brown, Justice Carbajal, Yevgen Chebotar, Xi Chen, Krzysztof Choromanski, Tianli Ding, Danny Driess, Avinava Dubey, Chelsea Finn, et al. Rt-2: Vision-language-action models transfer web knowledge to robotic control. *arXiv preprint arXiv:2307.15818*, 2023.
- Tom Brown, Benjamin Mann, Nick Ryder, Melanie Subbiah, Jared D Kaplan, Prafulla Dhariwal, Arvind Neelakantan, Pranav Shyam, Girish Sastry, Amanda Askell, et al. Language models are few-shot learners. *Advances in neural information processing systems*, 33:1877–1901, 2020.
- Ting Chen, Saurabh Saxena, Lala Li, David J Fleet, and Geoffrey Hinton. Pix2seq: A language modeling framework for object detection. *arXiv preprint arXiv:2109.10852*, 2021.
- Jaemin Cho, Jie Lei, Hao Tan, and Mohit Bansal. Unifying vision-and-language tasks via text generation. In *International Conference on Machine Learning*, pp. 1931–1942. PMLR, 2021.
- Aakanksha Chowdhery, Sharan Narang, Jacob Devlin, Maarten Bosma, Gaurav Mishra, Adam Roberts, Paul Barham, Hyung Won Chung, Charles Sutton, Sebastian Gehrmann, et al. Palm: Scaling language modeling with pathways. *arXiv preprint arXiv:2204.02311*, 2022.
- Hyung Won Chung, Le Hou, Shayne Longpre, Barret Zoph, Yi Tay, William Fedus, Eric Li, Xuezhi Wang, Mostafa Dehghani, Siddhartha Brahma, et al. Scaling instruction-finetuned language models. *arXiv preprint arXiv:2210.11416*, 2022.
- Sudeep Dasari and Abhinav Gupta. Transformers for one-shot visual imitation. In *Conference on Robot Learning*, pp. 2071–2084. PMLR, 2021.

- Jacob Devlin, Ming-Wei Chang, Kenton Lee, and Kristina Toutanova. Bert: Pre-training of deep bidirectional transformers for language understanding. *arXiv preprint arXiv:1810.04805*, 2018.
- Alexey Dosovitskiy, Lucas Beyer, Alexander Kolesnikov, Dirk Weissenborn, Xiaohua Zhai, Thomas Unterthiner, Mostafa Dehghani, Matthias Minderer, Georg Heigold, Sylvain Gelly, et al. An image is worth 16x16 words: Transformers for image recognition at scale. *arXiv preprint arXiv:2010.11929*, 2020.
- Danny Driess, Fei Xia, Mehdi SM Sajjadi, Corey Lynch, Aakanksha Chowdhery, Brian Ichter, Ayzan Wahid, Jonathan Tompson, Quan Vuong, Tianhe Yu, et al. Palm-e: An embodied multi-modal language model. *arXiv preprint arXiv:2303.03378*, 2023.
- Linda Drijvers and Judith Holler. The multimodal facilitation effect in human communication. *Psychonomic Bulletin & Review*, 30(2):792–801, 2023.
- Yonathan Efroni, Dipendra Misra, Akshay Krishnamurthy, Alekh Agarwal, and John Langford. Provable rl with exogenous distractors via multistep inverse dynamics. *arXiv preprint arXiv:2110.08847*, 2021.
- Francesco Giuliari, Irtiza Hasan, Marco Cristani, and Fabio Galasso. Transformer networks for trajectory forecasting. In *2020 25th international conference on pattern recognition (ICPR)*, pp. 10335–10342. IEEE, 2021.
- Pierre-Louis Guhur, Shizhe Chen, Ricardo Garcia Pinel, Makarand Tapaswi, Ivan Laptev, and Cordelia Schmid. Instruction-driven history-aware policies for robotic manipulations. In *Conference on Robot Learning*, pp. 175–187. PMLR, 2023.
- Kaiming He, Haoqi Fan, Yuxin Wu, Saining Xie, and Ross Girshick. Momentum contrast for unsupervised visual representation learning. In *Proceedings of the IEEE/CVF conference on computer vision and pattern recognition*, pp. 9729–9738, 2020.
- Wenlong Huang, Pieter Abbeel, Deepak Pathak, and Igor Mordatch. Language models as zero-shot planners: Extracting actionable knowledge for embodied agents. In *International Conference on Machine Learning*, pp. 9118–9147. PMLR, 2022a.
- Wenlong Huang, Fei Xia, Ted Xiao, Harris Chan, Jacky Liang, Pete Florence, Andy Zeng, Jonathan Tompson, Igor Mordatch, Yevgen Chebotar, et al. Inner monologue: Embodied reasoning through planning with language models. *arXiv preprint arXiv:2207.05608*, 2022b.
- Andrew Jaegle, Felix Gimeno, Andy Brock, Oriol Vinyals, Andrew Zisserman, and Joao Carreira. Perceiver: General perception with iterative attention. In *International conference on machine learning*, pp. 4651–4664. PMLR, 2021.
- Yunfan Jiang, Agrim Gupta, Zichen Zhang, Guanzhi Wang, Yongqiang Dou, Yanjun Chen, Li Fei-Fei, Anima Anandkumar, Yuke Zhu, and Linxi Fan. Vima: General robot manipulation with multimodal prompts. In *Fortieth International Conference on Machine Learning*, 2023.
- Alex Lamb, Riashat Islam, Yonathan Efroni, Aniket Rajiv Didolkar, Dipendra Misra, Dylan J Foster, Lekan P Molu, Rajan Chari, Akshay Krishnamurthy, and John Langford. Guaranteed discovery of control-endogenous latent states with multi-step inverse models. *Transactions on Machine Learning Research*, 2022.
- Shuang Li, Xavier Puig, Chris Paxton, Yilun Du, Clinton Wang, Linxi Fan, Tao Chen, De-An Huang, Ekin Akyürek, Anima Anandkumar, et al. Pre-trained language models for interactive decision-making. *Advances in Neural Information Processing Systems*, 35:31199–31212, 2022.
- Ilya Loshchilov and Frank Hutter. Decoupled weight decay regularization. *arXiv preprint arXiv:1711.05101*, 2017.
- Jiasen Lu, Christopher Clark, Rowan Zellers, Roozbeh Mottaghi, and Aniruddha Kembhavi. Unified-io: A unified model for vision, language, and multi-modal tasks. *arXiv preprint arXiv:2206.08916*, 2022.

- Corey Lynch and Pierre Sermanet. Language conditioned imitation learning over unstructured data. *arXiv preprint arXiv:2005.07648*, 2020.
- OpenAI. Gpt-4 technical report. *ArXiv*, abs/2303.08774, 2023. URL <https://api.semanticscholar.org/CorpusID:257532815>.
- Long Ouyang, Jeffrey Wu, Xu Jiang, Diogo Almeida, Carroll Wainwright, Pamela Mishkin, Chong Zhang, Sandhini Agarwal, Katarina Slama, Alex Ray, et al. Training language models to follow instructions with human feedback. *Advances in Neural Information Processing Systems*, 35: 27730–27744, 2022.
- Deepak Pathak, Pulkit Agrawal, Alexei A Efros, and Trevor Darrell. Curiosity-driven exploration by self-supervised prediction. In *International conference on machine learning*, pp. 2778–2787. PMLR, 2017.
- Alec Radford, Karthik Narasimhan, Tim Salimans, Ilya Sutskever, et al. Improving language understanding by generative pre-training. *OpenAI Blog*, 2018.
- Alec Radford, Jong Wook Kim, Chris Hallacy, Aditya Ramesh, Gabriel Goh, Sandhini Agarwal, Girish Sastry, Amanda Askell, Pamela Mishkin, Jack Clark, et al. Learning transferable visual models from natural language supervision. In *International conference on machine learning*, pp. 8748–8763. PMLR, 2021.
- Ilija Radosavovic, Baifeng Shi, Letian Fu, Ken Goldberg, Trevor Darrell, and Jitendra Malik. Robot learning with sensorimotor pre-training. *arXiv preprint arXiv:2306.10007*, 2023.
- Colin Raffel, Noam Shazeer, Adam Roberts, Katherine Lee, Sharan Narang, Michael Matena, Yanqi Zhou, Wei Li, and Peter J Liu. Exploring the limits of transfer learning with a unified text-to-text transformer. *The Journal of Machine Learning Research*, 21(1):5485–5551, 2020.
- Scott Reed, Konrad Zolna, Emilio Parisotto, Sergio Gomez Colmenarejo, Alexander Novikov, Gabriel Barth-Maron, Mai Gimenez, Yury Sulsky, Jackie Kay, Jost Tobias Springenberg, et al. A generalist agent. *arXiv preprint arXiv:2205.06175*, 2022.
- Victor Sanh, Albert Webson, Colin Raffel, Stephen H Bach, Lintang Sutawika, Zaid Alyafeai, Antoine Chaffin, Arnaud Stiegler, Teven Le Scao, Arun Raja, et al. Multitask prompted training enables zero-shot task generalization. *arXiv preprint arXiv:2110.08207*, 2021.
- Rutav Shah, Roberto Martín-Martín, and Yuke Zhu. Mutex: Learning unified policies from multimodal task specifications. In *7th Annual Conference on Robot Learning*, 2023. URL <https://openreview.net/forum?id=PwqiqaaEzJ>.
- Mohit Shridhar, Lucas Manuelli, and Dieter Fox. Perceiver-actor: A multi-task transformer for robotic manipulation. In *Conference on Robot Learning*, pp. 785–799. PMLR, 2023.
- Ilya Sutskever, Oriol Vinyals, and Quoc V Le. Sequence to sequence learning with neural networks. *Advances in neural information processing systems*, 27, 2014.
- Garrett Thomas, Ching-An Cheng, Ricky Loynd, Vibhav Vineet, Mihai Jalobeanu, and Andrey Kolobov. Plex: Making the most of the available data for robotic manipulation pretraining. *arXiv preprint arXiv:2303.08789*, 2023.
- Hugo Touvron, Thibaut Lavril, Gautier Izacard, Xavier Martinet, Marie-Anne Lachaux, Timothée Lacroix, Baptiste Rozière, Naman Goyal, Eric Hambro, Faisal Azhar, et al. Llama: Open and efficient foundation language models. *arXiv preprint arXiv:2302.13971*, 2023.
- Maria Tsimpoukelli, Jacob L Menick, Serkan Cabi, SM Eslami, Oriol Vinyals, and Felix Hill. Multimodal few-shot learning with frozen language models. *Advances in Neural Information Processing Systems*, 34:200–212, 2021.
- Ashish Vaswani, Noam Shazeer, Niki Parmar, Jakob Uszkoreit, Llion Jones, Aidan N Gomez, Łukasz Kaiser, and Illia Polosukhin. Attention is all you need. *Advances in neural information processing systems*, 30, 2017.

- David Venuto, Sherry Yang, Pieter Abbeel, Doina Precup, Igor Mordatch, and Ofir Nachum. Multi-environment pretraining enables transfer to action limited datasets. In *International Conference on Machine Learning*, pp. 35024–35036. PMLR, 2023.
- Oriol Vinyals, Igor Babuschkin, Junyoung Chung, Michael Mathieu, Max Jaderberg, Wojtek Czarnecki, Andrew Dudzik, Aja Huang, Petko Georgiev, Richard Powell, Timo Ewalds, Dan Horgan, Manuel Kroiss, Ivo Danihelka, John Agapiou, Junhyuk Oh, Valentin Dalibard, David Choi, Laurent Sifre, Yury Sulsky, Sasha Vezhnevets, James Molloy, Trevor Cai, David Budden, Tom Paine, Caglar Gulcehre, Ziyu Wang, Tobias Pfaff, Toby Pohlen, Dani Yogatama, Julia Cohen, Katrina McKinney, Oliver Smith, Tom Schaul, Timothy Lillicrap, Chris Apps, Koray Kavukcuoglu, Demis Hassabis, and David Silver. AlphaStar: Mastering the Real-Time Strategy Game StarCraft II. <https://deepmind.com/blog/alphastar-mastering-real-time-strategy-game-starcraft-ii/>, 2019.
- Wenhui Wang, Hangbo Bao, Li Dong, Johan Bjorck, Zhiliang Peng, Qiang Liu, Kriti Aggarwal, Owais Khan Mohammed, Saksham Singhal, Subhojit Som, et al. Image as a foreign language: Beit pretraining for all vision and vision-language tasks. *arXiv preprint arXiv:2208.10442*, 2022.
- Jason Wei, Maarten Bosma, Vincent Y Zhao, Kelvin Guu, Adams Wei Yu, Brian Lester, Nan Du, Andrew M Dai, and Quoc V Le. Finetuned language models are zero-shot learners. *arXiv preprint arXiv:2109.01652*, 2021.
- Andy Zeng, Pete Florence, Jonathan Tompson, Stefan Welker, Jonathan Chien, Maria Attarian, Travis Armstrong, Ivan Krasin, Dan Duong, Vikas Sindhwani, et al. Transporter networks: Rearranging the visual world for robotic manipulation. In *Conference on Robot Learning*, pp. 726–747. PMLR, 2021.

Appendix

A INDIVIDUAL TASK SUCCESS RATE OF DIFFERENT METHODS

In this section, we support all experimental results in Sec. 4 of our main paper with individual task success rates for all four levels of evaluation protocol. Specifically, the results for Table 1 and the ablation on Pretraining strategies can be found in Table 3, 4, 5 and 6. Figure 7 that ablates multimodal prompt encoding is based on the results from Table 7, 8, 9 and 10. The results in Figure 8 that ablate model and data sizes are based on the results from Table 11, 12, 13, 14, 15, 16, 17, and 18.

Additionally, we further conduct an ablation study on the transformer architecture of our policy by replacing the decoder-only architecture with encoder-decoder architecture (Our Method w/ Encoder-Decoder). Experimental results in Table 3, 4, 5 and 6 show that this variant does not perform as well as our method on the L1, L2, and L3 tasks, mainly due to its inability to tackle Task 09 (*Twist*) that requires deducting rotation angles from the prompt image sequence (Figure 2). However, it achieves a superior performance on the L4 Task 10 (*Follow Motion*). We hypothesize that it is due to the limit of model capacity. This policy learns a control policy that predicts its action dependent on the object bounding box, while lacking the capability to capture fine-grained visual information that contains the information of object rotation.

Table 3: L1 level generalization results. All methods share the same amount of parameters 92M. Integers in the first row refer to indices of tasks defined in the VIMA paper (Jiang et al., 2023)

Method	T1	T2	T3	T4	T5	T6	T7	T9	T11	T12	T15	T16	T17	Overall
VIMA	100	100	100	100	65.0	99.5	100	13.5	96.0	94.5	100	88.0	77.0	87.2
Gato OBJ	100	100	100	100	75.5	100	100	16.5	88.5	93.0	100	92.5	80.0	88.2
Our Method w/o Pretrain	100	100	100	98.5	88.0	100	100	20.5	100	94.0	99.0	93.0	98.0	91.6
w/ Pretrain	98.5	100	100	99.5	94.0	100	100	100	100	94.0	95.5	94.0	96.5	97.8
w/ Masked Pretrain	100	99.5	100	99.5	97.5	99.5	100	17.5	74.5	94.5	97.0	42.5	96.5	86.0
w/ Encoder-Decoder	100	100	99.5	99.5	96.5	100	100	19.5	99.5	93.5	99.0	93.0	82.5	91.0

Table 4: L2 level generalization results. All methods share the same amount of parameters 92M. Integers in the first row refer to indices of tasks defined in the VIMA paper (Jiang et al., 2023).

Method	T1	T2	T3	T4	T5	T6	T7	T9	T11	T12	T15	T16	T17	Overall
VIMA	100	100	100	99.5	61.0	100	100	12.5	97.5	95.0	100	87.5	77.5	87.0
Gato OBJ	100	100	100	100	73.0	100	100	17.5	88.5	95.0	99.0	94.0	80.5	88.3
Our Method w/o Pretrain	100	100	100	99.0	87.0	100	100	23.5	100	94.0	99.5	92.0	98.0	91.8
w/ Pretrain	98.5	100	100	99.0	96.5	99.5	100	100	100	95.5	95.0	93.0	96.0	97.9
w/ Masked Pretrain	99.5	100	100	99.5	96.5	100	99.5	19.5	75.5	95.5	97.0	43.5	96.5	86.3
w/ Encoder-Decoder	99.5	100	99.0	99.5	96.5	100	100	15.5	99.5	94.0	98.5	92.0	82.5	90.5

Table 5: L3 level generalization results. All methods share the same amount of parameters 92M. Integers in the first row refer to indices of tasks defined in the VIMA paper (Jiang et al., 2023).

Method	T1	T2	T3	T4	T5	T6	T7	T9	T11	T15	T16	T17	Overall
VIMA	99.5	100	100	99.5	63.0	99.5	100	12.0	98.5	99.5	58.5	78.0	84.0
Gato OBJ	99.5	100	100	100	72.5	97.5	100	7.5	95.0	99.5	44.5	72.0	82.3
Our Method w/o Pretrain	99.5	100	100	100	90.0	100	100	20.5	100	99.5	50.5	99.5	88.3
w/ Pretrain	98.0	99.0	100	99.5	94.0	97.5	99.0	97.0	96.5	95.0	47.0	98.0	93.4
w/ Masked Pretrain	99.0	100	100	100	96.5	99.5	99.0	20.5	76.5	99.0	42.0	100	86.0
w/ Encoder-Decoder	99.0	99.5	100	98.5	95.5	99.5	98.0	20.0	100	95.0	56.0	86.0	87.2

Table 6: L4 level generalization results. All methods share the same amount of parameters 92M. Integers in the first row refer to indices of tasks defined in the VIMA paper (Jiang et al., 2023).

Method	T8	T10	T13	T14	Overall
VIMA	98.5	0.0	0.0	100	49.6
Gato OBJ	99.5	0.0	0.0	98.0	49.4
Our Method					
w/o Pretrain	97.0	0.0	0.0	99.5	49.1
w/ Pretrain	97.5	41.0	1.0	97.0	59.1
w/ Masked Pretrain	95.0	0.0	0.0	99.0	48.5
w/ Encoder-Decoder	96.5	85.5	0.0	97.0	69.8

Table 7: Comparison of the performance of our method with different multimodal prompt encoder on L1 level generalization. All methods share the same amount of parameters 92M. Integers in the first row refer to indices of tasks defined in the VIMA paper (Jiang et al., 2023)

Pretrain iter.	Method	T1	T2	T3	T4	T5	T6	T7	T9	T11	T12	T15	T16	T17	Overall
0.0K	T5 + RC (Ours)	100	100	100	98.5	88.0	100	100	20.5	100	94.0	99.0	93.0	98.0	91.6
0.0K	T5	100	99.5	98.5	99.0	84.5	100	100	16.0	100	94.5	98.0	49.5	97.0	87.4
0.0K	VL-T5	100	100	98.5	99.5	66.0	100	100	18.0	100	93.0	96.5	94.0	96.0	89.3
3.1K	T5 + RC (Ours)	100	100	100	98.5	85.5	100	99.0	52.0	100	93.5	96.0	93.0	96.0	93.3
3.1K	T5	100	100	100	100	98.5	100	100	18.5	100	93.5	97.0	43.5	96.5	88.3
3.1K	VL-T5	100	99.5	100	100	70.0	99.5	100	23.5	100	94.5	99.5	43.5	96.5	86.7
5.2K	T5 + RC (Ours)	100	100	100	99.0	92.0	99.5	100	99.5	100	95.5	95.0	93.0	97.0	97.7
5.2K	T5	100	100	100	98.5	98.0	100	100	19.5	100	94.0	98.5	42.0	96.5	88.2
5.2K	VL-T5	100	99.5	100	99.0	94.0	99.5	99.5	21.0	100	94.0	95.5	43.0	96.5	87.8
10.3K	T5 + RC (Ours)	98.5	100	100	99.5	94.0	100	100	100	100	94.0	95.5	94.0	96.5	97.8
10.3K	T5	99.5	99.5	100	97.0	98.0	99.0	99.5	22.0	100	94.0	99.5	41.0	97.0	88.2
10.3K	VL-T5	99.5	99.0	100	100	97.5	99.0	100	100	100	93.5	98.0	43.0	97.0	94.3

Table 8: Comparison of the performance of our method with different multimodal prompt encoder on L2 level generalization. All methods share the same amount of parameters 92M. Integers in the first row refer to indices of tasks defined in the VIMA paper (Jiang et al., 2023)

Pretrain iter.	Method	T1	T2	T3	T4	T5	T6	T7	T9	T11	T12	T15	T16	T17	Overall
0.0K	T5 + RC (Ours)	100	100	100	99.0	87.0	100	100	23.5	100	94.0	99.5	92.0	98.0	91.8
0.0K	T5	99.5	100	99.0	99.5	87.0	100	99.5	20.0	100	93.5	98.5	48.0	95.0	87.7
0.0K	VL-T5	100	100	98.5	99.0	66.5	99.0	99.5	19.0	100	94.0	96.5	92.0	95.0	89.2
3.1K	T5 + RC (Ours)	99.5	100	100	98.5	89.5	100	99.5	52.0	100	94.0	92.5	92.0	96.0	93.3
3.1K	T5	99.0	100	100	100	97.0	99.0	99.5	22.5	100	94.5	96.0	41.5	96.5	88.1
3.1K	VL-T5	98.0	99.5	99.5	98.5	67.5	99.0	99.5	24.0	100	94.0	96.5	44.0	95.5	85.8
5.2K	T5 + RC (Ours)	100	100	100	97.5	91.0	98.5	99.5	99.5	100	95.5	93.0	92.5	96.5	97.2
5.2K	T5	98.5	100	100	98.0	96.5	99.0	98.5	21.5	100	94.0	93.5	40.0	95.0	87.3
5.2K	VL-T5	99.5	100	100	98.5	94.0	98.5	97.5	20.0	100	94.0	94.0	43.5	96.5	87.4
10.3K	T5 + RC (Ours)	98.5	100	100	99.0	96.5	99.5	100	100	100	95.5	95.0	93.0	96.0	97.9
10.3K	T5	100	100	100	97.0	97.0	100	97.0	19.5	100	94.5	97.0	43.0	95.0	87.7
10.3K	VL-T5	99.0	99.5	100	99.5	97.0	99.0	99.0	99.5	100	94.5	97.5	43.0	95.5	94.1

Table 9: Comparison of the performance of our method with different multimodal prompt encoder on L3 level generalization. All methods share the same amount of parameters 92M. Integers in the first row refer to indices of tasks defined in the VIMA paper (Jiang et al., 2023)

Pretrain iter.	Method	T1	T2	T3	T4	T5	T6	T7	T9	T11	T15	T16	T17	Overall
0.0K	T5 + RC (Ours)	99.5	100	100	100	90.0	100	100	20.5	100	99.5	50.5	99.5	88.3
0.0K	T5	98.5	98.5	100	100	85.5	99.5	98.5	19.5	100	98.5	42.0	57.5	83.2
0.0K	VL-T5	98.5	98.5	100	100	68.5	99.5	100	21.5	100	99.0	54.5	99.5	86.6
3.1K	T5 + RC (Ours)	97.0	98.0	99.0	99.0	90.5	96.0	99.5	45.5	98.0	97.0	47.5	96.5	88.6
3.1K	T5	96.0	99.0	99.5	100	98.0	97.0	96.0	21.5	100	95.5	42.0	99.5	87.0
3.1K	VL-T5	96.5	97.0	99.5	99.5	69.0	94.5	95.0	21.0	99.5	96.5	42.0	100	84.2
5.2K	T5 + RC (Ours)	99.5	99.0	100	99.0	93.0	98.0	99.0	98.0	98.0	95.5	46.0	97.0	93.5
5.2K	T5	96.5	96.0	99.5	100	97.5	98.5	97.0	17.5	100	97.0	38.5	100	86.5
5.2K	VL-T5	96.0	98.5	99.5	100	96.5	95.5	95.5	21.0	100	98.0	41.5	100	86.8
10.3K	T5 + RC (Ours)	98.0	99.0	100	99.5	94.0	97.5	99.0	97.0	96.5	95.0	47.0	98.0	93.4
10.3K	T5	99.0	97.5	100	99.5	96.5	96.0	95.0	15.5	100	95.5	43.5	99.5	86.5
10.3K	VL-T5	98.0	97.0	100	99.5	96.0	97.0	96.5	84.5	100	99.5	41.0	99.5	92.4

Table 10: Comparison of the performance of our method with different multimodal prompt encoder on L4 level generalization. All methods share the same amount of parameters 92M. Integers in the first row refer to indices of tasks defined in the VIMA paper (Jiang et al., 2023)

Pretrain iter.	Method	T8	T10	T13	T14	Overall
0.0K	T5 + RC (Ours)	97.0	0.0	0.0	99.5	49.1
0.0K	T5	95.0	0.0	0.0	98.5	48.4
0.0K	VL-T5	99.0	0.0	0.0	97.5	49.1
3.1K	T5 + RC (Ours)	97.5	12.5	0.0	98.5	52.1
3.1K	T5	98.0	45.0	0.0	95.5	59.6
3.1K	VL-T5	98.5	64.0	0.0	96.0	64.6
5.2K	T5 + RC (Ours)	98.0	40.5	0.0	96.5	58.8
5.2K	T5	98.5	55.5	0.0	96.0	62.5
5.2K	VL-T5	98.0	37.5	0.0	96.5	58.0
10.3K	T5 + RC (Ours)	97.5	41.0	1.0	97.0	59.1
10.3K	T5	98.5	39.5	0.0	98.5	59.1
10.3K	VL-T5	97.5	53.5	0.0	98.0	62.3

Table 11: Comparison of the performance of our method with different model sizes ranging from 2M to 92M on L1 level generalization results. Integers in the first row refer to indices of tasks defined in the VIMA paper (Jiang et al., 2023)

Model size.	Method	T1	T2	T3	T4	T5	T6	T7	T9	T11	T12	T15	T16	T17	Overall
2M	Ours w/o Pretrain	100	98.5	99.0	89.5	48.5	100	100	19.5	97.0	91.0	98.0	36.0	24.0	77.0
2M	Ours	99.5	99.0	97.5	99.0	67.5	100	99.5	18.5	91.5	93.0	99.0	38.0	64.5	82.0
4M	Ours w/o Pretrain	100	100	99.5	97.0	55.0	100	100	18.0	96.0	95.0	99.5	44.0	40.0	80.3
4M	Ours	100	100	86.5	99.0	63.5	99.5	100	20.5	92.0	95.5	98.0	83.5	57.0	84.2
9M	Ours w/o Pretrain	100	100	96.0	99.0	57.0	100	100	23.0	98.0	94.0	98.5	47.0	94.0	85.1
9M	Ours	100	100	99.0	99.0	87.0	100	100	19.0	100	95.5	98.5	92.5	97.0	91.3
20M	Ours w/o Pretrain	100	100	100	98.5	67.5	100	100	30.5	98.5	95.0	99.0	49.5	85.0	86.4
20M	Ours	100	100	100	97.0	90.0	100	99.5	19.0	100	94.0	99.5	93.5	97.5	91.5
43M	Ours w/o Pretrain	100	100	100	98.5	67.0	100	100	17.0	100	94.0	99.0	92.5	96.5	89.6
43M	Ours	99.5	100	99.5	95.5	89.0	97.5	100	100	100	94.5	96.0	94.5	96.5	97.1
92M	Ours w/o Pretrain	100	100	100	98.5	88.0	100	100	20.5	100	94.0	99.0	93.0	98.0	91.6
92M	Ours	98.5	100	100	99.5	94.0	100	100	100	100	94.0	95.5	94.0	96.5	97.8

Table 12: Comparison of the performance of our method with different model sizes ranging from 2M to 92M on L2 level generalization results. Integers in the first row refer to indices of tasks defined in the VIMA paper (Jiang et al., 2023)

Model size.	Method	T1	T2	T3	T4	T5	T6	T7	T9	T11	T12	T15	T16	T17	Overall
2M	Ours w/o Pretrain	95.5	84.5	99.0	87.0	50.0	96.5	91.0	21.0	97.0	91.0	88.0	33.5	11.5	72.7
	Ours	99.5	98.5	98.5	98.5	59.0	100	98.5	20.5	92.0	92.5	99.0	39.5	61.5	81.3
4M	Ours w/o Pretrain	99.0	98.5	100	97.0	55.0	99.5	98.5	21.0	96.5	95.5	97.0	44.0	35.0	79.7
	Ours	100	100	87.0	99.0	67.5	99.5	99.5	19.0	92.5	95.5	97.0	84.0	60.0	84.7
9M	Ours w/o Pretrain	100	100	96.5	98.5	58.0	99.5	99.0	25.5	97.5	94.5	94.5	47.0	88.0	84.5
	Ours	100	100	99.5	98.5	86.5	99.5	100	19.0	100	94.5	97.0	91.5	95.0	90.8
20M	Ours w/o Pretrain	100	100	100	98.5	72.0	100	100	29.5	98.0	95.5	99.0	46.0	83.5	86.3
	Ours	100	100	100	97.0	86.5	99.0	99.0	19.5	100	95.0	97.0	91.5	96.5	90.8
43M	Ours w/o Pretrain	100	100	100	98.5	72.5	100	100	18.5	100	93.5	99.5	92.0	96.0	90.0
	Ours	99.0	100	100	97.0	90.5	98.0	100	99.5	100	95.5	94.0	93.0	96.5	97.2
92M	Ours w/o Pretrain	100	100	100	99.0	87.0	100	100	23.5	100	94.0	99.5	92.0	98.0	91.8
	Ours	98.5	100	100	99.0	96.5	99.5	100	100	100	95.5	95.0	93.0	96.0	97.9

Table 13: Comparison of the performance of our method with different model sizes ranging from 2M to 92M on L3 level generalization results. Integers in the first row refer to indices of tasks defined in the VIMA paper (Jiang et al., 2023)

Model size.	Method	T1	T2	T3	T4	T5	T6	T7	T9	T11	T15	T16	T17	Overall
2M	Ours w/o Pretrain	97.0	91.0	100	92.5	46.0	96.5	95.5	15.5	95.5	95.0	36.0	8.0	72.4
	Ours	99.0	98.5	99.5	99.5	67.0	99.5	99.5	16.5	83.5	98.5	33.5	54.0	79.0
4M	Ours w/o Pretrain	98.5	98.0	100	94.5	53.5	95.0	99.0	17.0	99.0	87.5	47.0	5.5	74.5
	Ours	95.5	99.0	75.5	95.5	61.0	95.5	96.5	19.0	92.5	79.5	42.0	32.0	73.6
9M	Ours w/o Pretrain	93.5	97.5	96.0	100	64.0	95.0	96.0	17.5	97.5	85.0	43.0	44.0	77.4
	Ours	97.0	97.0	100	96.5	86.0	99.0	99.0	23.5	98.5	96.0	52.5	100	87.1
20M	Ours w/o Pretrain	99.5	100	100	100	71.5	100	100	26.0	98.5	98.5	43.5	87.5	85.4
	Ours	97.0	97.0	99.5	99.5	89.0	98.0	98.0	24.0	100	99.0	53.5	98.0	87.7
43M	Ours w/o Pretrain	99.5	100	100	100	74.0	100	99.5	25.0	100	99.5	54.0	99.0	87.5
	Ours	95.0	98.0	99.5	96.5	86.0	95.5	96.5	97.0	99.5	96.0	40.0	99.0	91.5
92M	Ours w/o Pretrain	99.5	100	100	100	90.0	100	100	20.5	100	99.5	50.5	99.5	88.3
	Ours	98.0	99.0	100	99.5	94.0	97.5	99.0	97.0	96.5	95.0	47.0	98.0	93.4

Table 14: Comparison of the performance of our method with different model sizes ranging from 2M to 92M on L4 level generalization results. Integers in the first row refer to indices of tasks defined in the VIMA paper (Jiang et al., 2023)

Model size.	Method	T8	T10	T13	T14	Overall
2M	Ours w/o Pretrain	78.5	0.0	0.0	95.5	43.5
	Ours	47.5	35.5	0.5	97.5	45.2
4M	Ours w/o Pretrain	99.5	0.0	0.0	95.5	48.8
	Ours	96.0	0.5	0.0	92.5	47.2
9M	Ours w/o Pretrain	96.5	1.0	0.0	95.0	48.1
	Ours	99.5	15.5	0.5	98.0	53.4
20M	Ours w/o Pretrain	99.0	0.0	0.0	99.0	49.5
	Ours	97.0	22.0	0.0	95.5	53.6
43M	Ours w/o Pretrain	99.0	0.0	0.0	98.5	49.4
	Ours	95.5	6.0	0.0	96.0	49.4
92M	Ours w/o Pretrain	97.0	0.0	0.0	99.5	49.1
	Ours	97.5	41.0	1.0	97.0	59.1

Table 15: Comparison of the performance of our method with different scales of training data on L1 level generalization results. Integers in the first row refer to indices of tasks defined in the VIMA paper (Jiang et al., 2023)

Data Size	Method	T1	T2	T3	T4	T5	T6	T7	T9	T11	T12	T15	T16	T17	Overall
10%	Ours w/o Pretrain	100	98.5	96.5	97.0	74.0	97.5	100	19.0	100	93.0	93.0	88.0	93.0	88.4
10%	Ours	100	99.5	96.5	89.0	65.5	98.0	98.5	73.5	97.5	93.5	92.0	89.0	93.0	91.2
50%	Ours w/o Pretrain	100	99.5	97.5	98.0	74.0	99.5	99.5	20.0	100	92.5	98.0	82.0	91.0	88.6
50%	Ours	100	99.5	98.5	98.0	86.5	99.5	99.5	98.5	100	93.5	96.5	95.5	96.5	97.1
100%	Ours w/o Pretrain	100	100	100	98.5	88.0	100	100	20.5	100	94.0	99.0	93.0	98.0	91.6
100%	Ours	98.5	100	100	99.5	94.0	100	100	100	100	94.0	95.5	94.0	96.5	97.8

Table 16: Comparison of the performance of our method with different scales of training data on L2 level generalization results. Integers in the first row refer to indices of tasks defined in the VIMA paper (Jiang et al., 2023)

Data Size	Method	T1	T2	T3	T4	T5	T6	T7	T9	T11	T12	T15	T16	T17	Overall
10%	Ours w/o Pretrain	99.5	99.0	97.0	95.5	72.5	97.5	99.5	20.5	98.5	93.0	91.5	88.5	91.0	88.0
10%	Ours	99.0	99.5	94.5	90.0	62.5	98.5	99.0	77.5	98.5	94.0	90.0	87.0	89.0	90.7
50%	Ours w/o Pretrain	98.5	100	97.0	98.0	72.0	99.5	99.5	16.5	100	91.5	97.5	84.5	88.5	87.9
50%	Ours	100	100	99.0	97.5	88.5	99.0	99.0	98.5	100	95.0	96.0	95.5	96.5	97.3
100%	Ours w/o Pretrain	100	100	100	99.0	87.0	100	100	23.5	100	94.0	99.5	92.0	98.0	91.8
100%	Ours	98.5	100	100	99.0	96.5	99.5	100	100	100	95.5	95.0	93.0	96.0	97.9

Table 17: Comparison of the performance of our method with different scales of training data on L3 level generalization results. Integers in the first row refer to indices of tasks defined in the VIMA paper (Jiang et al., 2023)

Data Size	Method	T1	T2	T3	T4	T5	T6	T7	T9	T11	T15	T16	T17	Overall
10%	Ours w/o Pretrain	98.0	97.0	97.5	98.5	74.5	97.5	99.0	18.0	100	96.5	53.5	99.0	85.8
10%	Ours	90.0	93.5	98.5	93.0	71.0	90.0	90.5	56.0	90.0	83.0	52.0	20.5	77.3
50%	Ours w/o Pretrain	97.5	99.5	99.0	99.5	70.5	98.5	99.0	19.0	100	97.0	57.5	93.5	85.9
50%	Ours	97.0	97.5	99.0	99.5	86.0	97.5	96.5	95.5	98.0	97.0	47.5	100	92.6
100%	Ours w/o Pretrain	99.5	100	100	100	90.0	100	100	20.5	100	99.5	50.5	99.5	88.3
100%	Ours	98.0	99.0	100	99.5	94.0	97.5	99.0	97.0	96.5	95.0	47.0	98.0	93.4

Table 18: Comparison of the performance of our method with different scales of training data on L4 level generalization results. Integers in the first row refer to indices of tasks defined in the VIMA paper (Jiang et al., 2023)

Data Size	Method	T8	T10	T13	T14	Overall
10%	Ours w/o Pretrain	92.0	0.0	0.0	94.5	46.6
10%	Ours	91.0	39.0	0.0	88.0	54.5
50%	Ours w/o Pretrain	91.5	0.0	0.0	97.0	47.1
50%	Ours	95.0	12.5	0.0	96.0	50.9
100%	Ours w/o Pretrain	97.0	0.0	0.0	99.5	49.1
100%	Ours	97.5	41.0	1.0	97.0	59.1

B PSEUDO-CODES & TRAINING DETAILS

Algorithm 1 Robot Control with multimodal prompts through pretraining and multitask FT

Input: Dataset $\mathcal{D} = \{\zeta_1, \zeta_2, \dots\}$, policy parameter θ , number of pretraining iterations N_{pretrain} , number of multi-task imitation finetuning iterations N_{FT}

- 1: **for** $i = 1, \dots, N_{\text{pretrain}}$ **do**
 - 2: Sample a mini-batch \mathcal{B} from \mathcal{D}
 - 3: Minimize $L_{\text{pretrain}}(\theta)$ defined in Eq. 3 on \mathcal{B}
 - 4: **end for**
 - 5: **for** $i = 1, \dots, N_{\text{FT}}$ **do**
 - 6: Sample a mini-batch \mathcal{B} from \mathcal{D}
 - 7: Minimize $L_{\text{imitation}}(\theta)$ defined in Eq. 4 on \mathcal{B}
 - 8: **end for**
-

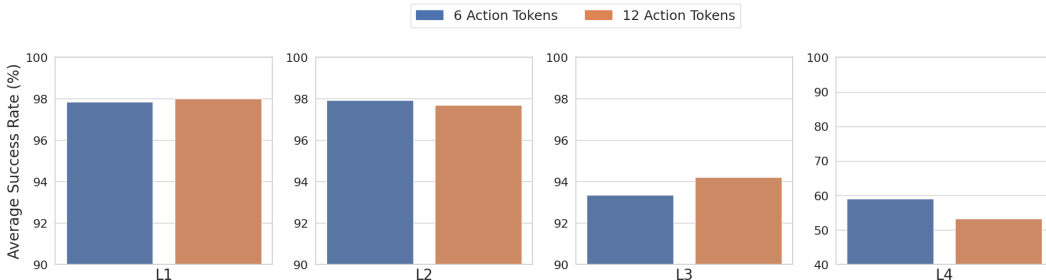


Figure 9: Ablation on the number of action tokens.

Algorithm 1 presents the pseudo-codes for the training pipeline, which includes a pretraining phase and a multi-task FT phase. We set our training HP following the recipe provided by VIMA, which open-sourced its policy architectures without providing the training codes. We conduct our experiments on cluster nodes, each with 8 NVIDIA-A10G. Table 19 presents the HP for our training pipeline. As we build our policy based on the VIMA Policy, we refer interested readers to Tables 2 and 3 in Appendix C of VIMA paper (Jiang et al., 2023) for all model parameters.

Additionally, the action space \mathcal{A} includes initial pose $\mathcal{T}_{\text{initial}} \in \mathcal{R}^6$ and $\mathcal{T}_{\text{target}} \in \mathcal{R}^6$. Each pose is a 6-dimension vector with 2 for xy position and 4 for rotation represented in quaternion. Since the VIMA-BENCH focuses on tabletop manipulation, the rotation quaternion of $\mathcal{T}_{\text{initial}}$ is always a constant vector. So is the first two dimensions of the rotation quaternion of $\mathcal{T}_{\text{initial}}$. Therefore, we only tokenize the other 6 action dimensions to improve computational efficiency. Thus, each action worth 6 tokens. Moreover, we conduct an ablation study to show that this choice will not affect the task success rate. As shown in Figure 9, modeling each of the 12 action dimensions as a single token achieves almost the same performance as modeling the 6 active action dimensions.

Table 19: Hyper-parameters for our training pipeline

Phase	Hyperparameter	Value
Shared	Learning Rate (LR)	1e-4
	Minimum LR	1e-7
	Warmup Steps	7K
	Weight Decay	0
	Dropout	0.1
	Gradient Clip Threshold	1.0
	Optimizer	AdamW (Loshchilov & Hutter, 2017)
	Batch Size	128
	Iterations per epochs	5158
Pretrain	Training epochs	20
	Training iterations N_{pretrain}	$20 \times \text{Iterations per epochs} = 103160$
	LR Cosine Annealing Steps	$N_{\text{pretrain}} - \text{Warmup Steps} = 96160$
Finetune	LR Cosine Annealing Steps	17K
	Training epochs	10
	Training iterations N_{FT}	$10 \times \text{Iterations per epochs} = 51580$

C DETAILS OF EVALUATING THE IN-CONTEXT LEARNING ABILITY

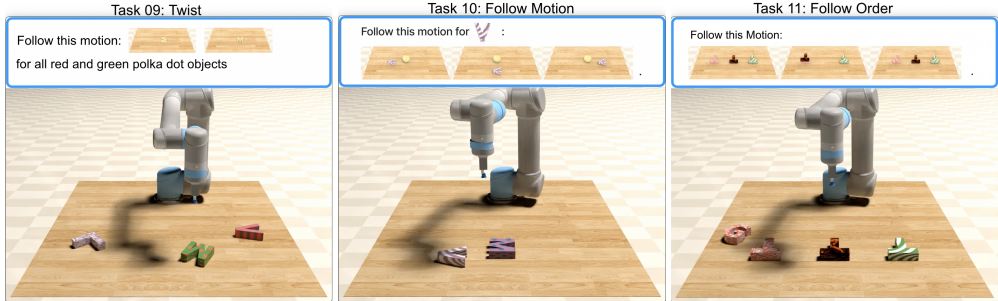


Figure 10: The new set of L4 tasks with in-context examples and modified prompts.

We provide training details for the experiments conducted in Sec. 4.3 by introducing the data augmentation strategies, pretraining, our *Modified FT*, and how we edit the task prompt for Task 09 (*Twist*) and Task 10 (*Follow Order*). Moreover, the L1, L2 and L3 success rate in this settings are given by 97.6%, 97.7%, and 93.0%, respectively.

Data Augmentation To improve the generalizability of the pretrained model, we randomly apply the standard random data augmentation techniques, including Color Jitter and Gray Scale (He et al., 2020) to the prompt images. Since we adopt an object-centric representation, we randomly shift the bounding box location for all objects in the whole trajectory with the same constant value. Note that we only augment the prompt images without modifying the observation images.

Pretraining We empirically find that further dividing the pretraining phase into two steps can improve the performance. We first pretrain a policy for 20 epochs and only extract the object encoder from it. Next, we use the pretrained object encoder to initialize another policy and pretrain it for 5 epochs. And the FT phase remains unchanged.

Modified FT To improve the model’s ability to understand both visual and textual object descriptions, we randomly replace the object images in the multimodal prompts with text descriptions during multi-task FT. For example, the task prompt for *Follow Motion* in Figure 10 can be rephrased as

Follow this motion for the white and purple striped V: {frame₁}, {frame₂}, {frame₃}.

Note that only object images will be converted into text descriptions. Images depicted the scene, e.g., frame₁, frame₂, frame₃, will never be converted to text. We randomly apply this operation to the task prompt of the pretraining tasks during the FT phase.

Edit Prompts As shown in Figure 10, we modify the task prompt for both *Twist* and *Follow order* to make them similar to the pretraining prompts. Specifically, the task prompt for *Twist* is modified as below

Original: “Twist” is defined as rotating object a specific angle. For examples: From {before_twist₁} to {after_twist₁}. From {before_twist₂} to {after_twist₂}. From {before_twist₃} to {after_twist₃}. Now twist all [TEXT OBJ DESCRIPTION] objects.

Modified: Follow this motion: {before_twist₁} to {after_twist₁} for all [TEXT OBJ DESCRIPTION] objects.

Similarly, the task prompt for *Follow Order* is modified as below:

Original: Stack objects in this order {frame₁}, {frame₂}, {frame₃}.

Modified: Follow this motion: {frame₁}, {frame₂}, {frame₃}.

D ADDITIONAL L4 UNSEEN TASKS WITH IN-CONTEXT EXAMPLES

We augment the L4 task suite of VIMA-BENCH by designing 4 new tasks with in-context examples provided in the prompt. These tasks are within the *One-shot Video Imitation* category of VIMA-BENCH (Appendix B.4, Jiang et al. (2023)). Next, we will first provide the task definitions. Then, we take our policy that is trained on the full data of VIMA-BENCH and evaluate it on these tasks. Notably, we never use trajectories collected from these tasks to train our policy.

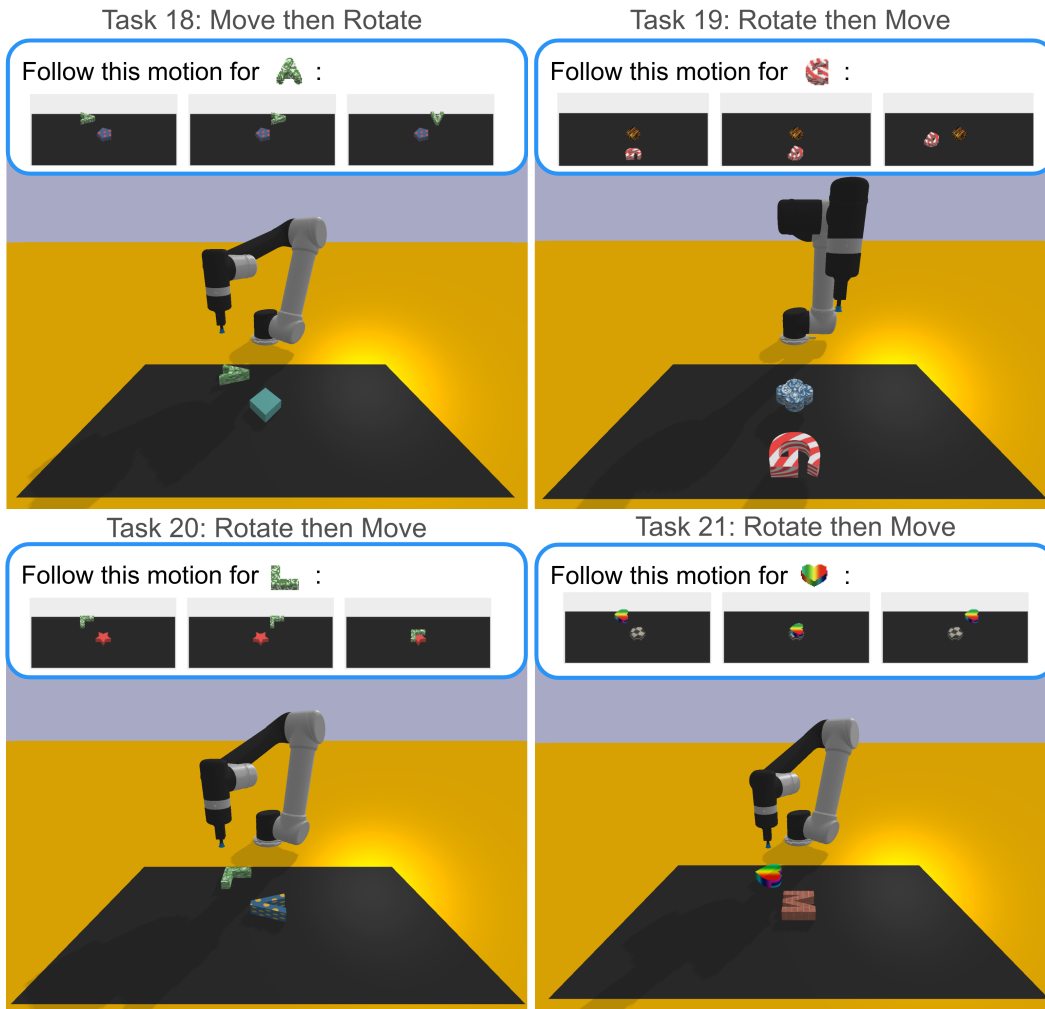


Figure 11: Task samples from our designed tasks. Each task is paired with in-context demonstration in the prompt.

D.1 TASK DEFINITION

To evaluate the in-context learning ability of a policy, we design four tasks to incorporate a demonstration trajectory in the task prompt. Specifically, these tasks share the same prompt template

Follow this motion for {target object}: {frame₁}, {frame₂}, {frame₃}.

Note that we did not inject language variety to the task prompt, **as we can always paraphrase the task prompt to the unified prompt defined above given demonstration trajectory.**

Image placeholder {target object} is the target object to be manipulated and {{frame_i}} a set of workspace-like scene placeholders to represent a video trajectory. Distractor objects are spawned

at the center of the workspace and the prompt video. However, the distractor in the workspace is different from the distractor in the prompt video. The initial position of the target object matches that in $\{\text{frame}_1\}$.

Task 18: Move then Rotate. The robot should first move the target object to a specific location and then rotate the target object by a certain degree, according to the demonstration trajectory.

Task 19: Rotate then Move. The robot should first rotate the target object by a certain degree and then move the target object to a specific location according to the demonstration trajectory.

Task 20: Move then Stack. The robot should first stack the target object on the distractor and then move the target object to a specific location according to the demonstration trajectory.

Task 21: Rotate then Move. The robot should first move the target object to a specific location and then stack the target object on the distractor according to the demonstration trajectory.

D.2 EXPERIMENTAL RESULTS ON THE UNSEEN TASKS

Table 20: Evaluating the in-context learning capability of the learned model on the four unseen tasks proposed in Appendix D.1. All policies are trained on the full data of VIMA-BENCH.

Method	Task 18	Task 19	Task 20	Task 21	Overall
Our Method	13.5%	14.5%	22.0%	10.0%	15.0%
Our Method w/ Pretrain Only	4.5%	0.5%	20.5%	1.5%	5.3%
Our Method w/o Pretrain	0.0%	0.0%	0.0%	0.5%	0.1%
VIMA	0.0%	0.0%	0.0%	0.5%	0.1%

We take policies trained on the full VIMA-BENCH data and directly compare their performance on these four new tasks. As shown in Table 20, Our Method significantly outperforms the baseline methods. On the other hand, the VIMA policy struggles to perform well on these tasks, showing its inability to learn from the in-context demonstration. Moreover, comparing the performance of Our Method with Our Method w/ Pretrain Only, we can conclude that our two-stage training pipeline produces a better in-context learner.